arXiv:1111.6894v1 [astro-ph.SR] 29 Nov 2011

Oscillatory large-scale dynamos from Cartesian convection simulations

P. J. KÄPYLÄ†‡* M. J. MANTERE† and A. BRANDENBURG‡§

†Physics Department, Gustaf Hällströmin katu 2a, FI-00014 University of Helsinki, Finland
‡NORDITA, Roslagstullsbacken 23, SE-10691 Stockholm, Sweden
§Department of Astronomy, Stockholm University, SE-10691 Stockholm, Sweden

We present results from compressible Cartesian convection simulations with and without imposed shear. In the former case the dynamo is expected to be of $\alpha^2\Omega$ type which is likely to be relevant for the Sun, whereas the latter case refers to α^2 dynamos which are more likely to occur in more rapidly rotating stars. The latter exhibit oscillatory large-scale magnetic fields. We perform a parameter study where the shear flow is kept fixed and the rotational influence is varied in order to probe the relative importance of both modes. We find that in cases with shear, the streamwise component of the magnetic field is between 9 and 20 times greater than the cross-streamwise one, depending on the rotation rate. Oscillatory solutions are preferred either when the shear is relatively strong or weak in comparison to rotation, but not when the two are comparable to each other. However, exceptions to these rules also appear and in many cases the solution is oscillatory only in the kinematic regime whereas in the nonlinear stage the mean fields are stationary. The cases with rotation and no shear are always oscillatory in the parameter range studied here and the dynamo mode does not depend on the magnetic boundary conditions. The strength of total and the large-scale component of the magnetic field at the saturated state, however, are sensitive to the chosen boundary conditions.

Keywords: Solar Dynamo, Convection, Turbulence

1 Introduction

The solar magnetic cycle is commonly thought to be a manifestation of an oscillatory large-scale dynamo operating within or just below the convection zone (e.g. Ossendrijver 2003). A possible origin of the solar magnetic fields is the turbulent dynamo mechanism, where helical small-scale fluid motions and large-scale shear sustain the magnetic field (e.g. Moffatt 1978, Krause and Rädler 1980, Rüdiger and Hollerbach 2004). According to mean-field theory, turbulent stratified convection together with global rotation of the Sun lead to an α effect (Steenbeck *et al.* 1966) and large-scale differential rotation (e.g. Rüdiger 1989). Their combined effect constitutes the $\alpha\Omega$-dynamo which often yields oscillatory solutions (e.g. Parker 1955, Steenbeck and Krause 1969).

However, reproducing the solar cycle with direct numerical simulations still remains challenging (e.g. Miesch and Toomre 2009, Käpylä 2011). Early spherical simulations were indeed able to achieve oscillatory large-scale fields that propagate toward the poles (Gilman 1983, Glatzmaier 1985). Simpler Cartesian models with rotating stratified convection were less successful as only small-scale fields were seen (e.g. Nordlund *et al.* 1992, Brandenburg *et al.* 1996). Only when a shear flow was added (Käpylä *et al.* 2008, Hughes and Proctor 2009) or rapid enough rotation was used (Jones and Roberts 2000, Rotvig and Jones 2002, Käpylä *et al.* 2009b), large-scale fields were obtained. Even in the cases with imposed shear, no oscillatory solutions were seen although the necessary prerequisites, helical turbulence and shear, were present. However, these are aspects that depend critically on the boundary conditions. Indeed, Käpylä *et al.* (2009c) have presented mean-field calculations of associated convection simulations that agree with each

---

*Corresponding author. Email: petri.kapyla@helsinki.fi

other not only qualitatively in that both are non-oscillatory, but they also agree quantitatively as far as their excitation condition is concerned.

Here we extend previous studies on large-scale dynamos due to turbulent convection in Cartesian geometry (Käpylä *et al.* 2008, 2009b) to cover a larger parameter space and to explore more thoroughly the effects of boundary conditions on the solutions. We present runs with imposed shear and find that oscillatory solutions can be found in a limited part of the parameter range studied. We also report on rigidly rotating runs where oscillatory α^2-dynamos are observed.

2   Model

Our model setup is the same as that of Käpylä *et al.* (2008, 2009b). A rectangular portion of a star is modelled with a box situated at colatitude θ. The dimensions of the computational domain are $(L_x, L_y, L_z) = (4, 4, 2)d$, where d is the depth of the convectively unstable layer, which is also used as the unit of length. The box is divided into three layers: an upper cooling layer, a convectively unstable layer, and a stable overshoot layer (see below). The following equations for compressible magnetohydrodynamics are solved:

$$\frac{\mathcal{D}\boldsymbol{A}}{\mathcal{D}t} = -SA_y\hat{\boldsymbol{x}} - (\boldsymbol{\nabla}\boldsymbol{U})^{\mathrm{T}}\boldsymbol{A} - \mu_0\eta\boldsymbol{J}, \tag{1}$$

$$\frac{\mathcal{D}\ln\rho}{\mathcal{D}t} = -\boldsymbol{\nabla}\cdot\boldsymbol{U}, \tag{2}$$

$$\frac{\mathcal{D}\boldsymbol{U}}{\mathcal{D}t} = -SU_x\hat{\boldsymbol{y}} - \frac{1}{\rho}\boldsymbol{\nabla}p + \boldsymbol{g} - 2\boldsymbol{\Omega}\times\boldsymbol{U} + \frac{1}{\rho}\boldsymbol{J}\times\boldsymbol{B} + \frac{1}{\rho}\boldsymbol{\nabla}\cdot 2\nu\rho\mathsf{S}, \tag{3}$$

$$\frac{\mathcal{D}e}{\mathcal{D}t} = -\frac{p}{\rho}\boldsymbol{\nabla}\cdot\boldsymbol{U} + \frac{1}{\rho}\boldsymbol{\nabla}\cdot K\boldsymbol{\nabla}T + 2\nu\mathsf{S}^2 + \frac{\mu_0\eta}{\rho}\boldsymbol{J}^2 - \frac{e-e_0}{\tau(z)}, \tag{4}$$

where $\mathcal{D}/\mathcal{D}t = \partial/\partial t + (\boldsymbol{U} + \overline{\boldsymbol{U}}_0)\cdot\boldsymbol{\nabla}$ is the advective derivative with respect to the total (turbulent plus shear) flow, $\overline{\boldsymbol{U}}_0 = (0, Sx, 0)$ is the imposed large-scale shear flow, $\boldsymbol{A}$ is the magnetic vector potential, $\boldsymbol{B} = \boldsymbol{\nabla}\times\boldsymbol{A}$ is the magnetic field, $\boldsymbol{J} = \boldsymbol{\nabla}\times\boldsymbol{B}/\mu_0$ is the current density, μ_0 is the magnetic permeability, η and ν are the magnetic diffusivity and kinematic viscosity, respectively, K is the heat conductivity, ρ is the density, $\boldsymbol{U}$ is the velocity, $\boldsymbol{g} = -g\hat{\boldsymbol{z}}$ is the gravitational acceleration, and $\boldsymbol{\Omega} = \Omega_0(-\sin\theta, 0, \cos\theta)$ is the rotation vector. The fluid obeys an ideal gas law $p = \rho e(\gamma - 1)$, where p and e are the pressure and internal energy, respectively, and $\gamma = c_{\mathrm{P}}/c_{\mathrm{V}} = 5/3$ is the ratio of specific heats at constant pressure and volume, respectively. The specific internal energy per unit mass is related to the temperature via $e = c_{\mathrm{V}}T$. The traceless rate of strain tensor S is given by

$$\mathsf{S}_{ij} = \tfrac{1}{2}(U_{i,j} + U_{j,i}) - \tfrac{1}{3}\delta_{ij}\boldsymbol{\nabla}\cdot\boldsymbol{U}. \tag{5}$$

The last term of Eq. (4) describes cooling at the top of the domain. Here, $\tau(z)$ is a cooling time which has a profile smoothly connecting the upper cooling layer and the convectively unstable layer below, where $\tau^{-1}(z) \to 0$.

The positions of the bottom of the box, bottom and top of the convectively unstable layer, and the top of the box, respectively, are given by $(z_1, z_2, z_3, z_4) = (-0.85, 0, 1, 1.15)d$. Initially the stratification is piecewise polytropic with polytropic indices $(m_1, m_2, m_3) = (3, 1, 1)$, which leads to a convectively unstable layer above a stable layer at the bottom of the domain and an isothermal cooling layer at the top. All simulations with rotation use $\theta = 0$, corresponding to the north pole.

2.1 *Nondimensional units and parameters*

Dimensionless quantities are obtained by setting

$$d = g = \rho_0 = c_{\mathrm{P}} = \mu_0 = 1 , \tag{6}$$

where ρ_0 is the initial density at z_2. The units of length, time, velocity, density, entropy, and magnetic field are

$$[x] = d , \quad [t] = \sqrt{d/g} , \quad [U] = \sqrt{dg} , \quad [\rho] = \rho_0 , \quad [s] = c_{\mathrm{P}} , \quad [B] = \sqrt{dg\rho_0\mu_0} . \tag{7}$$

We define the fluid and magnetic Prandtl numbers and the Rayleigh number as

$$\mathrm{Pr} = \frac{\nu}{\chi_0} , \quad \mathrm{Pm} = \frac{\nu}{\eta} , \quad \mathrm{Ra} = \frac{gd^4}{\nu\chi_0}\left(-\frac{1}{c_{\mathrm{P}}}\frac{\mathrm{d}s}{\mathrm{d}z} \right)_0 , \tag{8}$$

where $\chi_0 = K/(\rho_{\mathrm{m}}c_{\mathrm{P}})$ is the thermal diffusivity, and ρ_{m} is the density in the middle of the convectively unstable layer, $z_{\mathrm{m}} = z_3 - z_2$. The entropy gradient, measured at z_{m} in the non-convecting hydrostatic state, is given by

$$\left(-\frac{1}{c_{\mathrm{P}}}\frac{\mathrm{d}s}{\mathrm{d}z} \right)_0 = \frac{\nabla - \nabla_{\mathrm{ad}}}{H_{\mathrm{P}}} , \tag{9}$$

where $\nabla - \nabla_{\mathrm{ad}}$ is the superadiabatic temperature gradient with $\nabla_{\mathrm{ad}} = 1 - 1/\gamma$, $\nabla = (\partial \ln T/\partial \ln p)_{z_{\mathrm{m}}}$, where H_{P} is the pressure scale height. The amount of stratification is determined by the parameter $\xi_0 = (\gamma - 1)e_0/gd$, which is the pressure scale height at the top of the domain normalized by the depth of the unstable layer. We use $\xi_0 = 0.3$ in all cases, which results in a density contrast of about 23. We define the fluid and magnetic Reynolds numbers via

$$\mathrm{Re} = \frac{u_{\mathrm{rms}}}{\nu k_{\mathrm{f}}} , \quad \mathrm{Rm} = \frac{u_{\mathrm{rms}}}{\eta k_{\mathrm{f}}} , \tag{10}$$

where $k_{\mathrm{f}} = 2\pi/d$ is assumed as a reasonable estimate for the wavenumber of the energy-carrying eddies. Note that, according to this definition, Rm is by a factor 2π smaller than the usually adopted one based on d instead of k_{f}. The amounts of shear and rotation are quantified by

$$\mathrm{Sh} = \frac{S}{u_{\mathrm{rms}}k_{\mathrm{f}}} , \quad \mathrm{Co} = \frac{2\,\Omega_0}{u_{\mathrm{rms}}k_{\mathrm{f}}} . \tag{11}$$

The denominators in Eq. (11) give an estimate of the convective turnover time. We also use the value of the relative shear rate

$$q = -S/\Omega_0, \tag{12}$$

which is more often used in the context of disk systems, for which the local angular velocity varies like $\Omega_0 \propto r^{-q}$. The equipartition magnetic field is defined by

$$B_{\mathrm{eq}} \equiv \langle \mu_0 \rho \boldsymbol{U}^2 \rangle^{1/2}, \tag{13}$$

where angle brackets denote volume averaging.

2.2   *Boundary conditions*

Stress-free boundary conditions are used for the velocity,

$$U_{x,z} = U_{y,z} = U_z = 0, \tag{14}$$

and either vertical field or perfect conductor conditions for the magnetic field, i.e.

$$B_x = B_y = 0 \ \ \text{(vertical field)}, \tag{15}$$

$$B_{x,z} = B_{y,z} = B_z = 0 \ \ \text{(perfect conductor)}, \tag{16}$$

respectively. We may think of them as open and closed boundaries, respectively, because they either do or do not permit a magnetic helicity flux. In the y and x directions we use periodic and shearing-periodic boundary conditions, respectively. In the runs with shear and rotation we always use vertical field conditions at the top and perfect conductor conditions at the bottom. The simulations have been made with the PENCIL CODE[1], which uses sixth-order explicit finite differences in space and a third order accurate time stepping method.

3   Results

We perform two sets of simulations with shear and rotation (Sets A and B) and a few exploratory runs with only rotation (Set C), see Table 1. In the runs with shear we keep the shear rate S constant and vary the rotation rate Ω_0. In Set A we use $S = -0.05\sqrt{g/d}$ and in Set B we have $S = -0.1\sqrt{g/d}$. Hydrodynamical progenitors of the runs in Set A were used in Käpylä *et al.* (2010b) and the runs in Set B were obtained by doubling both S and Ω_0. In terms of q, we explore the range $-10 \ldots 1.99$. Values of q near zero refer to runs with rapid (and nearly rigid) rotation, whereas small values of $|q|$ are associated with slow rotation. For $q \geq 2$ the flow is Rayleigh unstable and thus we limit our study to values $q \leq 1.99$. The case where $S \neq 0$ and $\Omega_0 = 0$ is another special case in that a 'vorticity dynamo' (e.g. Elperin *et al.* 2003, Käpylä *et al.* 2009a) is excited for the values of shear chosen here. We also omit this part of the parameter regime (see, however Käpylä *et al.* 2008). We take Runs A9 and A1 from Käpylä *et al.* (2011) as the hydrodynamical progenitors for our runs in Set C with only rotation.

In the following we discuss first the case with shear and study the behavior solutions for a range of values of q. We refer to these solutions as α–shear dynamos. We study separately the case without shear and refer to such solutions as α^2 dynamos. We focus here specifically on the case of oscillatory solutions.

3.1 α–*shear dynamos*

In our previous studies of convection-driven large-scale dynamos with shear (Käpylä *et al.* 2008, 2009b, 2010a), only non-oscillatory solutions were obtained. The large-scale field often had a different sign in the convectively unstable layer with respect to the stable overshoot layer, although solutions with a single sign have been obtained at low magnetic Reynolds numbers (see Fig. 5 of Käpylä *et al.* 2010a) and in cases where $\Omega_0 = 0$ (see Fig. 7 of Käpylä *et al.* 2008). Runs with sinusoidal shear and rotation also show non-oscillatory large-scale fields (Hughes and Proctor 2009, Käpylä *et al.* 2010c).

As is evident form Table 1, many of our current runs are also non-oscillatory; see Figure 1(a) for a representative result from Run A6. When q is increased from unity, the mean magnetic field begins to show reversals. This is particularly clear in the kinematic regime in Runs A1–A3. Cycles in the non-linear regime are more irregular and in some cases the dynamo mode changes to a non-oscillatory mode (Run B1). With $q < 0.25$, another oscillatory regime is found. These runs tend to show oscillations in the kinematic stage but often switch to a stationary mode in the non-linear regime; see the time evolution

---

[1]http://pencil-code.googlecode.com/

Table 1. Summary of the runs. In Sets A and B we use $\mathrm{Pr} = 1$, $\mathrm{Ra} = 10^6$, $\mathrm{Pm} = 1$, and grid resolution 128^3. Perfect conductor (vertical field) conditions for the magnetic field at the lower (upper) boundary are used. In Set C, Pm varies, $\mathrm{Pr} = 0.24$, $\mathrm{Ra} = 2 \cdot 10^6$, and grid resolution 256×128^2. The boundary conditions in Set C are listed in the rightmost column of the table. Oscillatory (osc) and stationary (sta) modes of the dynamo are denoted in the second column from right. Question marks indicate that only very few sign changes are covered by the time series or irregular reversals are seen. Here, $\tilde{B}_{\mathrm{rms}} = B_{\mathrm{rms}}/B_{\mathrm{eq}}$, where B_{rms} is the total rms magnetic field, and $\overline{\tilde{B}}_i = \langle \overline{B}_i^2 \rangle^{1/2}/B_{\mathrm{eq}}$.

Run	Ma	Rm	q	Co	Sh	$\tilde{B}_{\mathrm{rms}}$	$\overline{\tilde{B}}_x$	$\overline{\tilde{B}}_y$	Mode	Comment
A1	0.031	25	1.99	0.26	−0.25	1.50	0.07	1.38	osc/osc?	
A2	0.029	23	1.75	0.31	−0.27	1.50	0.08	1.27	osc/osc	
A3	0.028	22	1.50	0.38	−0.28	1.58	0.10	1.29	osc/osc	
A4	0.027	22	1.25	0.46	−0.29	1.41	0.10	1.12	osc?/osc?	
A4	0.027	22	1.25	0.46	−0.29	1.41	0.10	1.12	sta/osc?	
A5	0.028	22	1.00	0.57	−0.28	2.65	0.22	2.46	sta/sta	
A6	0.029	23	0.75	0.73	−0.27	3.34	0.29	3.16	sta/sta	
A7	0.030	24	0.50	1.07	−0.27	3.92	0.37	3.73	sta/sta	
A8	0.029	23	0.25	2.17	−0.27	4.34	0.47	4.08	sta/sta	
A9	0.026	20	0.10	6.19	−0.31	5.70	0.61	5.33	osc/sta	
A10	0.023	18	0.05	13.7	−0.34	7.07	0.75	6.53	osc/sta	
A11	0.011	8	−0.05	−30.2	−0.75	−	−	−	osc/−	not run to saturation
A12	0.016	13	−0.10	−9.87	−0.49	−	−	−	osc/−	not run to saturation
A13	0.056	45	−0.25	−1.13	−0.14	2.21	0.36	1.81	osc?/sta	
A14	0.062	49	−0.50	−0.52	−0.13	2.10	0.22	1.85	sta/sta	
A15	0.027	21	−1.00	−0.59	−0.30	−	−	−	sta/−	no dynamo
A16	0.028	23	−2.50	−0.22	−0.28	−	−	−	osc/−	no dynamo
A17	0.030	24	−5.00	−0.11	−0.26	−	−	−	osc/−	no dynamo
A18	0.036	28	−10.0	−0.04	−0.22	−	−	−	osc/−	no dynamo
B1	0.090	72	1.99	0.18	−0.18	1.15	0.09	1.00	osc/sta	
B2	0.040	32	1.75	0.46	−0.40	2.70	0.13	2.54	osc/osc?	
B3	0.039	31	1.50	0.54	−0.40	3.18	0.18	2.99	sta/sta	
B4	0.040	31	1.25	0.64	−0.40	3.22	0.20	3.03	sta/sta	
B5	0.042	33	1.00	0.77	−0.38	2.94	0.20	2.74	sta/sta	
B6	0.034	27	0.75	1.25	−0.47	3.79	0.34	3.57	sta/sta	
B7	0.038	31	0.50	1.66	−0.42	3.63	0.29	3.38	sta/sta	
B8	0.036	29	0.25	3.50	−0.44	4.00	0.33	3.68	osc/sta	
B9	0.029	23	0.10	11.0	−0.55	4.51	0.41	4.00	sta/sta	
B10	−	−	0.05	−	−	−	−	−	−	no convection
B11	−	−	−0.05	−	−	−	−	−	−	no convection
B12	0.011	8	−0.10	−30.2	−1.51	−	−	−	osc/−	marginal dynamo
B13	0.018	15	−0.25	−6.91	−0.86	−	−	−	osc?/−	not run to saturation
B14	0.086	69	−0.50	−0.74	−0.18	1.35	0.19	1.01	osc?/sta	
B15	0.094	75	−1.00	−0.34	−0.17	1.16	0.10	0.95	osc?/sta	
B16	0.030	24	−2.50	−0.43	−0.54	−	−	−	osc/−	marginal dynamo
B17	0.032	26	−5.00	−0.20	−0.50	1.44	0.06	1.20	osc/sta	
B18	0.035	28	−10.0	−0.09	−0.46	1.61	0.08	1.35	osc/sta	
C1	0.021	66	−	4.60	−	1.18	0.30	0.31	osc/osc	Pm = 2, pc/vf
C1b	0.025	39	−	3.85	−	0.36	0.09	0.09	osc/osc	Pm = 1, pc/vf
C1c	0.032	26	−	2.96	−	−	−	−	osc/−	Pm = 0.5, pc/vf, dynamo decays
C1d	0.021	66	−	4.60	−	1.18	0.32	0.29	osc/osc	Pm = 2, vf/vf
C1e	0.023	72	−	4.22	−	0.54	0.10	0.09	osc/osc	Pm = 2, pc/pc
C2	0.018	58	−	17.5	−	0.64	0.10	0.10	osc/osc	Pm = 2, pc/vf

of the horizontally averaged magnetic field components from Run B8 in Figure 1(b). We find that in the parameter regime explored here, non-oscillatory solutions are consistently found near $q = 1$. This explains the lack of oscillatory dynamos in our previous works where we always used $q = 1$. This further illustrates the importance of comprehensive parameter studies instead of individual numerical experiments (Käpylä *et al.* 2010b).

Many runs in the $q < 0$ regime, especially in Set A, are either subcritical or show very slow growth of the magnetic field and were not run to saturation. Convection is suppressed especially near $q = 0$ due to the rapid rotation, decreasing the Reynolds number and thus explaining the absence of dynamo action there. This can seem surprising because in the $q < 0$ regime the contributions to the α effect due to shear and rotation have the same sign (Käpylä *et al.* 2009b). On the other hand, the magnetorotational instability can be excited for $q > 0$ which may explain the more favourable dynamo excitation in that regime. However, we find that if a saturated dynamo is present in this regime, also the turbulence is enhanced (see Runs A13, A14, B14, and B15). This is associated with the generation of additional large-scale flows that depend on x, see Figure 4. Also the large-scale magnetic fields are x-dependent. Such modes are not
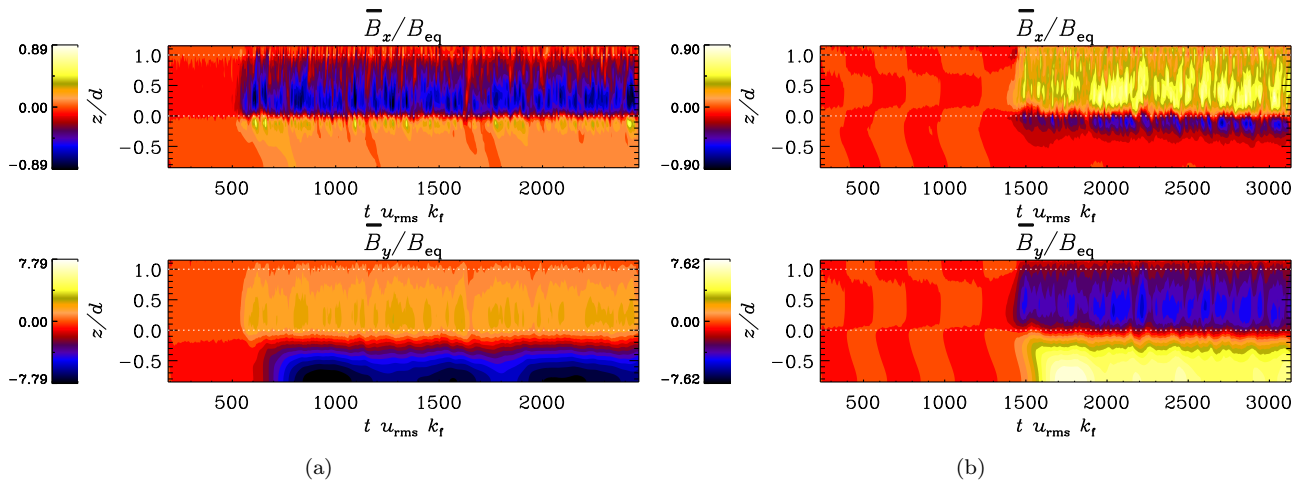
Figure 1. Horizontally averaged horizontal components of the magnetic field from non-oscillatory Run A6 (a) and initially oscillatory but ultimately stationary Run B8 (b) α-shear dynamos.

visible in the kinematic stages of the runs.

Even in the cases with the clearest oscillatory solutions, e.g. Run A2 in Fig. 2(a), the period of the oscillation varies from cycle to cycle. Furthermore, the cycle period is of the order of 10^3 convective turnover times in this run. Such a long cycle period limits the duration of the simulation to only a few cycles.

The cycle frequency of a saturated α–shear dynamo under the assumption of homogeneity is given by

$$\omega_{\mathrm{cyc}} = \eta_{\mathrm{T}} k_{\mathrm{m}}^2, \tag{17}$$

where $\eta_{\mathrm{T}} = \eta_{\mathrm{t}} + \eta$ is the total magnetic diffusivity, η_{t} is the turbulent diffusivity, and k_{m} is the wavenumber of the dominant mode of the magnetic field (Blackman and Brandenburg 2002). Because this is valid in the non-linear regime, the quenching of η_{t} as a function of Rm and $\overline{\boldsymbol{B}}$ can be estimated (Käpylä and Brandenburg 2009). However, such procedure is not directly applicable here due to inhomogeneity of the system and the fact that a number of other effects are also present (e.g. Käpylä *et al.* 2009c), rendering Eq. (17) inaccurate. However, provided that we are dealing with a turbulent dynamo, the cycle frequency is likely regulated by the value of η_{t}. This suggests that the turbulent diffusivity is quenched by a factor of roughly two to three in Run A2, compared to the kinematic stage of the same run.

The phase diagram of the horizontal components of the large-scale field averaged over $0.2d < z < 0.8d$ in Run A2 are shown in Fig. 3(a). The streamwise and cross-stream field components are in antiphase in this case.

3.2   *Oscillatory α^2 dynamos*

In an earlier study we found the appearance of large-scale magnetic fields in rigidly rotating convection (Käpylä *et al.* 2009b). However, none of the runs in that paper were run for much more than 10^3 convective turnover times. Although sign changes of the large-scale fields were seen (see, Fig. 7 of KKB09), the time series were too short to enable any firm conclusions regarding the possibly oscillatory nature of the dynamo.

Furthermore, in similar rapidly rotating runs without magnetic fields, the appearance of large-scale vortices has been discovered (Chan 2007, Käpylä *et al.* 2011, Mantere *et al.* 2011). Here we use the hydrodynamical states of runs with large-scale cyclones as initial conditions for our dynamo simulations. We find that a large-scale dynamo is excited provided the magnetic Reynolds number exceeds a certain critical value. Furthermore, as the magnetic fields become dynamically important, the cyclones decay and are absent in the non-linear state. The large-scale magnetic field is oscillatory in the two cases with different values of Co that we have considered. Figure 2(b) shows the horizontally averaged mean magnetic fields from a rigidly rotating Run C1 where an α^2 dynamo is excited. In Run C1 the large-scale fields are only
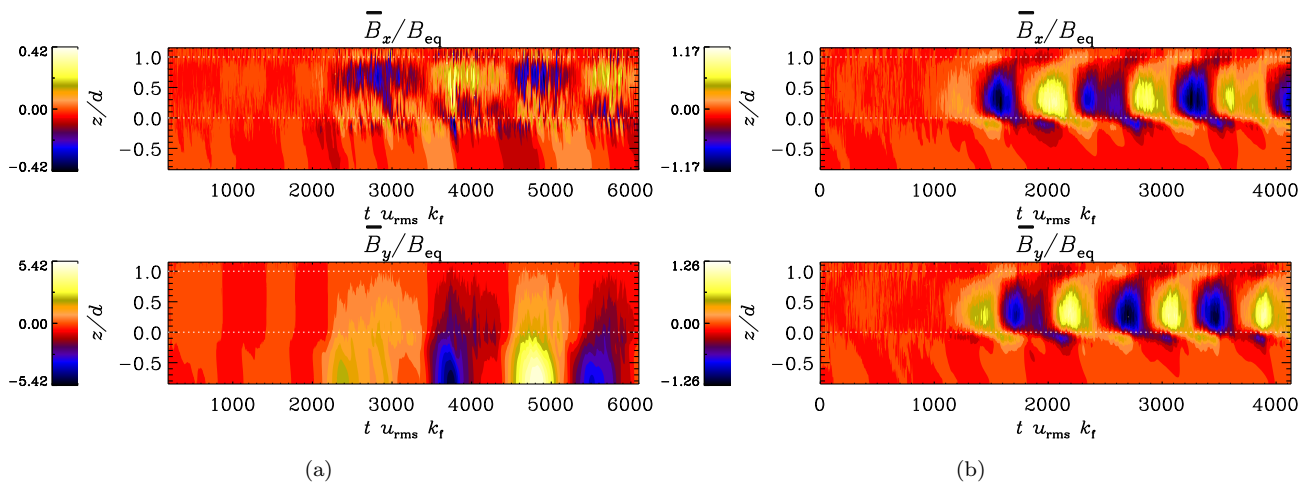
Figure 2. Same as Fig. 1 but for oscillatory α-shear dynamo Run A2 (a) and α^2 dynamo Run C1 (b).
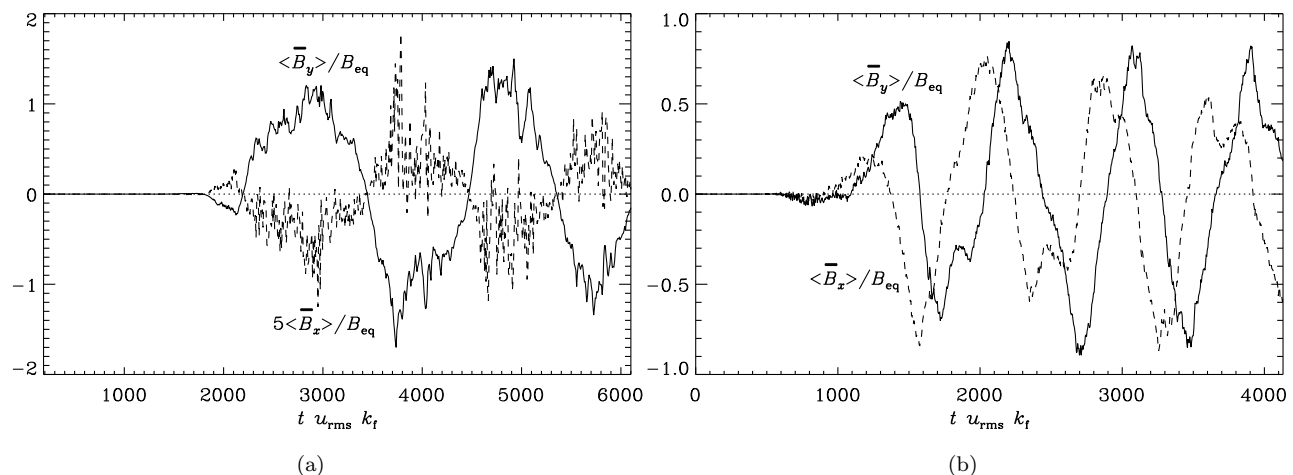

Figure 3. Phase diagrams for the same runs as in Fig. 2.

functions of z whereas in the more rapidly rotating Run C2 the large-scale fields depend also on x and y. Furthermore, the oscillatory nature of the solution is not so clear. Figure 3(b) shows the phase diagram of the horizontal components of the large-scale field in Run C1. There is a phase shift of $\pi/2$.

The saturation level of the dynamo is sensitive to the magnetic Reynolds number. Decreasing Rm from 66 to 39 by doubling the value of η, decreases the saturation field strength by a factor of three (Run C1b). Another doubling of η shuts the dynamo off (Run C1c).

Our standard setup in the present paper is to use perfect conductor boundaries at the bottom and vertical field conditions at the top. Changing also the lower boundary to vertical field conditions produces no discernible difference in the solution (Run C1d). However, imposing perfect conductor conditions on both boundaries decreases the saturation strength to less than a half of the standard setup and decreases the fraction of the large-scale field (Run C1e). We have not, however, studied the Rm-dependence of the saturation field strength in this case (cf. Käpylä *et al.* 2010a).

4   Conclusions

We have presented results from simulations of turbulent magnetized convection both with an imposed shear flow using the shearing box approximation (Sets A and B) and in rigidly rotating cases (Set C). In accordance with previous results, we find the generation of dynamically important large-scale magnetic
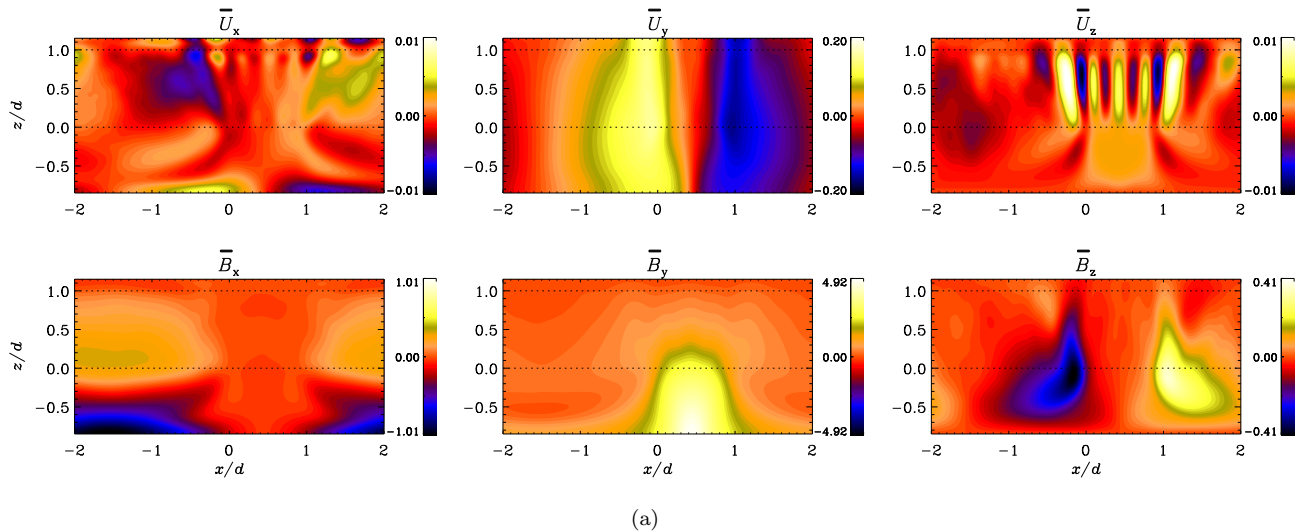
Figure 4.   Mean velocities (upper row) and magnetic fields (lower row) averaged over the y-direction and time from Run B14. The velocities are shown in units of $\sqrt{dg}$ and the magnetic fields in units of volume averaged equipartition field B_{eq}.

fields. In distinction to our earlier studies, we here vary the relative importance of rotation with respect to shear by covering the range $q = -10 \ldots 1.99$ of the relative shear rate q. We find that for $q = 1$ the solutions are always stationary, which is in accordance with earlier results. For large q, i.e. slower rotation, and for $q \ll 1$, oscillatory solutions are found. These trends are particularly clear in the kinematic regime. In the saturated state, however, we often find that the dynamo switches from oscillatory to stationary.

In the rigidly rotating cases of Set C, all the dynamo solutions are found to be oscillatory. Large-scale vortices, present in the hydrodynamic state, are no longer found in the saturated state of the dynamo. Usage of a perfect conductor boundary condition instead of a vertical field condition, allowing for magnetic helicity fluxes, is found to decrease both the total saturation field strength and the strength of the large-scale field with respect to the total magnetic field.

REFERENCES

Brandenburg, A., Jennings, R. L., Nordlund, Å., Rieutord, M., Stein, R. F. and Tuominen, I., Magnetic structures in a dynamo simulation. *J. Fluid Mech.* 1996, **306**, 325–352.

Blackman, E.G. and Brandenburg, A., Dynamic Nonlinearity in Large-Scale Dynamos with Shear. *Astrophys. J.* 2002, **579**, 359–373.

Chan, K.-L., Rotating convection in f-boxes: Faster rotation. *Astron. Nachr.* 2007, **328**, 1059–1062.

Elperin, T., Kleeorin, N. and Rogachevskii, I., Generation of large-scale vorticity in a homogeneous turbulence with a mean velocity shear. *Phys. Rev. E* 2003, **68**, 016311.

Gilman, P., Dynamically consistent nonlinear dynamos driven by convection in a rotating spherical shell. II - Dynamos with cycles and strong feedbacks. *Astrophys. J. Suppl.* 1983, **53**, 243–268.

Glatzmaier, G.A., Numerical simulations of stellar convective dynamos. II - Field propagation in the convection zone. *Astrophys. J.* 1985, **291**, 300–307.

Hughes, D.W. and Proctor, M.R.E., Large-Scale Dynamo Action Driven by Velocity Shear and Rotating Convection. *Phys. Rev. Lett.* 2009, **102**, 044501

Jones, C.A. and Roberts, P.H., Convection-driven dynamos in a rotating plane layer. *J. Fluid Mech.* 2000, **404**, 311–343.

Käpylä, P.J., Korpi, M.J. and Brandenburg, A., Large-scale dynamos in turbulent convection with shear. *Astron. Astrophys.* 2008, **491**, 353–362.

Käpylä, P.J. and Brandenburg, A., Turbulent dynamos with shear and fractional helicity. *Astrophys. J.* 2009, **699**, 1059–1066.

Käpylä, P.J., Mitra, D. and Brandenburg, A., Numerical study of large-scale vorticity generation in shear-flow turbulence. *Phys. Rev. E* 2009a, **79**, 016302.

Käpylä, P.J., Korpi, M.J. and Brandenburg, A., Large-scale Dynamos in Rigidly Rotating Turbulent Convection. *Astrophys. J.* 2009b, **697**, 1153–1163 (KKB09).

Käpylä, P.J., Korpi, M.J. and Brandenburg, A., Alpha effect and turbulent diffusion from convection. *Astron. Astrophys.* 2009c, **500**, 633–646.

Käpylä, P.J., Korpi, M.J. and Brandenburg, A., Open and closed boundaries in large-scale convective dynamos. *Astron. Astrophys.* 2010a, **518**, A22.

Käpylä, P.J., Brandenburg, A., Korpi, M.J., Snellman J.E. and Narayan, R., Angular momentum transport in convectively unstable shear flows. *Astrophys. J.* 2010b, **719**, 67–76.

Käpylä, P.J., Korpi, M.J. and Brandenburg, A., The α effect in rotating convection with sinusoidal shear. *Monthly Notices of the Roy. Astron. Soc.* 2010c, **402**, 1458–1466.

Käpylä, P.J., Mantere, M.J. and Hackman, T., Starspots due to large-scale vortices in rotating turbulent convection. *Astrophys. J.* 2011, **742**, 34.

Käpylä, P.J., On global solar dynamo simulations. *Astron. Nachr.* 2011, **332**, 43–50.

Krause, F. and Rädler, K.H., *Mean-field Magnetohydrodynamics and Dynamo Theory*, 1980 (Oxford: Pergamon Press).

Mantere, M.J., Käpylä, P.J. and Hackman, T., Dependence of the large-scale vortex instability on latitude, stratification and domain size. *Astron. Nachr.* 2011 (in press), arXiv:1109.4317

Miesch, M.S. and Toomre, J., Turbulence, Magnetism, and Shear in Stellar Interiors. *Annual Review of Fluid Mechanics* 2009, **41**, 317–345.

Moffatt, H.K., *Magnetic Field Generation in Electrically Conducting Fluids*, 1978 (Cambridge: Cambridge University Press).

Nordlund, Å., Brandenburg, A., Jennings, R. L., Rieutord, M., Ruokolainen, J., Stein, R. F. and Tuominen, I., Dynamo action in stratified convection with overshoot. *Astrophys. J.* 1992, **392**, 647–652.

Ossendrijver, M., The solar dynamo. *Astron. Astrophys. Rev.* 2003, **11**, 287–367.

Parker, E.N. Hydromagnetic Dynamo Models *Astrophys. J.* 1955, **121**, 491

Rotvig J. and Jones, C.A., Rotating convection-driven dynamos at low Ekman number. *Phys. Rev. E* 2002, **66**, 056308.

Rüdiger, G., *Differential Rotation and Stellar Convection. Sun and Solar-type Stars*, 1989 (Berlin: Akademie Verlag).

Rüdiger, G. and Hollerbach, R., *The Magnetic Universe: Geophysical and Astrophysical Dynamo Theory*, 2004 (Weinheim: Wiley-VCH).

Steenbeck, M., Krause, F. and Rädler, K.-H., Berechnung der mittleren Lorentz-Feldstärke für ein elektrisch leitendes Medium in turbulenter, durch Coriolis-Kräfte beeinflußter Bewegung. *Z. Naturforsch. A* 1966, **21**, 369

Steenbeck, M. and Krause, F., On the Dynamo Theory of Stellar and Planetary Magnetic Fields. I. AC Dynamos of Solar Type. *Astron. Nachr.* 1969, **291**, 49–84